DETERMINATION OF ELEVATOR AND RUDDER HINGE FORCES

ON THE LEARJET MODEL 55 AIRCRAFT

Robert R. Boroughs and Viswa Padmanabhan
Gates Learjet Corporation

SUMMARY

The empennage structure on the Learjet 55 aircraft was quite similar to the empennage structure on earlier Learjet models. However, due to an important structural change in the vertical fin along with the new loads environment on the 50 series aircraft, a structural test was required on the vertical fin, but the horizontal tail was substantiated by a comparative analysis with previous tests. NASTRAN analysis was used to investigate empennage deflections, stress levels, and control surface hinge forces. The hinge force calculations were made with the control surfaces in the deflected as well as undeflected configurations. A skin panel buckling analysis was also performed, and the non-linear effects of buckling were simulated in the NASTRAN model to more accurately define internal loads and stress levels. Comparisons were then made between the Model 55 and the Model 35/36 stresses and internal forces to determine which components were qualified by previous tests. Some of the methods and techniques used in this analysis have been described in the following paragraphs.

INTRODUCTION

Features in the 55 empennage section that were identical to previous Learjet models included the horizontal tail, elevators, and the upper portion of the vertical fin and rudder (see figure 1). The most significant change in the empennage occurred in the lower portion of the vertical fin and rudder which were expanded using the same taper ratio and airfoil contour as the upper portion so that the total height of the vertical fin and rudder was increased by approximately 15 inches. Since the vertical tail increased in size and the vertical fin spar depths and spacings changed at the intersection with the tailcone, an entirely new tailcone section was designed to support the empennage section. Control systems for the elevators and rudder were nearly the same as the previous controls in this area with the exception of the 15 inch height increase in the vertical tail and the geometry changes in the tailcone.

Construction in the vertical tail consisted of five spars and eight ribs made of bent up aluminum sheet metal covered with an aluminum skin. The rudder was assembled with one spar, eleven ribs, and a thin skin cover, all of which were aluminum sheet metal fabrication. Support for the rudder was accomplished through three hinge points. Two of these hinges, the top and center attachments, connected the rudder leading edge to the rear spar of the vertical stabilizer while the third hinge point, or bottom support, was attached to the aft side of frame 48 through a torque tube and bracket support assembly (see figure 2). Near the lower end of this torque tube was mounted a bellcrank assembly which provided the means for actuating and controlling the rudder surface.

Structural arrangement of the horizontal tail included a forward and rear spar with three intermediate stringers on both the upper and lower surfaces, seven ribs per side, and upper and lower skin panels. The elevators were one spar airfoil sections with nine ribs per side which were covered with an aluminum skin. Each elevator was attached to the horizontal stabilizer by three hinge points along the elevator leading edge. The tip and center span hinges both connected directly to the rear spar of the horizontal stabilizer, but the inboard hinge attachment was very similar to the lower hinge on the rudder. The elevator inboard hinge consisted of a torque tube assembly which was supported at the horizontal stabilizer rear spar and aircraft center line by a bracket assembly. This bracket installation served as a support for both the right hand and left hand elevators at the inboard end (see figure 3). Actuation and control of the elevators was achieved through individual bellcranks on the inboard end of each torque tube. These bellcrank assemblies were then connected by a push rod linkage system which extended through the vertical stabilizer to a control system sector in the fuselage tailcone.

SYMBOLS

A_i — X, Y, and Z components of a point at the origin for a CORD2R card

α — rotation about the x axis for element internal forces

B_i — X, Y, and Z components of a point on the Z axis for a CORD2R card

β — rotation about the Y axis for element internal forces

C_i — X, Y, and Z components of a point in the X-Z plane for a CORD2R card

F_{iE} — internal force component

γ — rotation about z axis for element internal forces

H_G — coordinate values of a deflected control surface transformed to the basic system

H_L — coordinate values of a deflected control surface in a local system

H_λ — coordinate values corrected for hinge line sweep

H_θ — coordinate values corrected for control surface rotation

λ — hinge line sweep

$T\lambda$ — transformation matrix for hinge line sweep

$T\theta$ — transformation matrix for control surface rotation

θ — control surface rotation

x — first coordinate of a point in a local rectangular system

y — second coordinate of a point in a local rectangular system

z   third coordinate of a point in a local rectangular system

X   first coordinate of a point in the basic rectangular system

Y   second coordinate of a point in the basic rectangular system

Z   third coordinate of a point in the basic rectangular system

BACKGROUND

Since the Model 55 empennage structure was very similar to the Model 35/36 empennage structure and other earlier empennage structures, Learjet was faced with the situation on the 50 series development program of determining which structural items were qualified by previous certification tests and which structural items needed to be requalified. The vertical tail and tailcone support structure was obviously one area which had to be qualified by structural test, since the height of this component had been increased on the 50 series aircraft. A portion of the NASTRAN analysis on that structure has been detailed in NASA CP-2151 (see ref. 1) and consequently has not been addressed in this text. However, a description of the NASTRAN analysis performed on the rudder and rudder hinges was not covered in that document and has been incorporated in the body of this paper.

A review of the loads for the 50 series aircraft helped to further clarify some of these questions, but for some structural components the answer was not obvious and more study was necessary. One area where this was particularly true was the horizontal tail installation. This situation was mainly due to a revised loads definition for the horizontal tail where the combination of new loads was not directly comparable to the older load conditions. Also, a faster method was needed for calculating elevator hinge forces for the various load conditions and deflected elevator configurations. Previously, hinge forces had been calculated using methods which were very tedious, time consuming, and not very adaptable to changes in elevator position.

To help clarify these questions a NASTRAN analysis was performed on the empennage structure for the various load conditions and control surface positions so that a comparison could be made between the deflections, stresses, and internal loads on the 55 empennage with the 35/36 empennage. Previous structural tests had demonstrated that the horizontal stabilizer and elevators on the 35/36 aircraft had the capability to sustain 150% of ultimate load (not limit load) for two of the more critical conditions on that airplane. The 150% of ultimate load tests were performed to more accurately define the strength of the horizontal stabilizer and elevators as well as establish the growth capability of this structure. Consequently, a portion of the NASTRAN analysis was spent simulating the 35/36 load conditions in order to establish a baseline for the 50 series analysis. Then the 50 series loads were applied to the NASTRAN model and a comparison was made between these data and the 35/36 data. Using this approach Learjet was able to more clearly define which elements were qualified by previous certification tests and which members, if any, need to be qualified in the 50 series substantiation program. This data base would also help to establish what components needed to be qualified in future growth versions and/or modifications to the existing configuration.

MODELING CRITERIA

The NASTRAN model used to represent the empennage section included the vertical stabilizer, rudder, horizontal stabilizer, elevators, and tailcone section (see figure 1). The tailcone was utilized in the model to more accurately describe the flexibility and stiffness of the vertical tail, since the spars from the vertical tail extended into and were attached to the tailcone. A significant portion of the control system connecting the rudder and elevators was also modeled to more accurately define the effect of control system flexibility on the deflection of the control surfaces and hinge forces.

Since this structure was geometrically quite complex, multiple local coordinate systems were used to simplify the modeling and to make the analysis easier to perform for the different control system deflected configurations. Each frame in the tailcone section was modeled in a local cylindrical coordinate system while the vertical fin and horizontal stabilizer were modeled in a local rectangular coordinate system. The rudder and elevators were all modeled in local rectangular systems with the Y axis of each coordinate system defined along the hinge line. This type of coordinate system definition permitted the rotation of each control surface about the hinge line by simply transforming the CORD2R card (see ref. 2) rather than changing all of the grid point coordinates in the control surface to reflect the deflected position. Rotation of the control surface about the hinge line thus permitted the calculation of hinge forces for various control surface movements. This technique also facilitated a study of vertical fin and horizontal stabilizer internal forces and stresses for various control surface positions.

The model for this structure was approximately 5700 degrees of freedom in size with 950 nodes and 2800 elements. Local coordinate systems totaled seventeen which consisted of both rectangular and cylindrical reference systems. Since the results of previous static tests had indicated that skin panel buckling was present, a buckling analysis was implemented to identify buckled skin panels and to simulate this non-linear phenomenon in the NASTRAN analysis (see ref. 3). This buckling simulation was achieved by replacing the original skin thickness of the buckled panel with an effective skin thickness which represented the stiffness of the buckled configuration. The buckling analysis and effective skin thickness calculation were performed by a computer program which was set up to run as a post processor to the NASTRAN program. This process generally had to be repeated several times in order to obtain a convergent solution. A more detailed description of the theory behind this analysis has been presented in NASA TMX 3428 and further discussion will not be covered in this text.

TAILCONE

Incorporation of the tailcone section with the empennage model was done to more accurately define the stiffness relationship between these two components. Representation of the tailcone section included the structure from frame 39 to frame 48 (see figure 1). The modeling of this structure was accomplished by defining the grid points at each frame and stringer intersection in a local cylindrical coordinate system in the plane of the frame using CORD2C cards (see ref. 2). NASTRAN members used to model this structure were BAR elements for the frames,

CONROD element ... skin and
doublers. A baggage door on the left hand side of the tailcone did not have sig-
nificant structural carry through capability and was omitted to conserve degrees
of freedom. The keel beam structure that extended from frame 39 to 41 in this
section was modeled using CONROD elements for the caps, SHEAR elements for the side
webs, and QDMEM2 elements for the horizontal webs.

VERTICAL TAIL

Two separate local rectangular coordinate systems were used to facilitate the
definition of grid point locations in the vertical fin and rudder (see figure 2).
The local rectangular coordinate system for the vertical fin was defined using a
CORD2R card with the origin located on the center line of the airplane at the inter-
section of the vertical tail leading edge and the tailcone upper surface. The X
axis was defined as positive aft, the Y axis was defined as positive up, and the Z
axis was defined as positive left hand outboard. The local rectangular coordinate
system for the rudder was defined using a CORD2R card with the origin on the rudder
hinge line at the lower end of the rudder torque tube. Orientation of the X axis
was positive aft and slightly down (for zero degree rudder deflection), the Y axis
was positive up along the rudder hinge line, and the Z axis was positive left hand
outboard.

Grid points were located at the intersection of the spar caps and rib caps
on both the right hand and left hand outer contours of the vertical tail. The
spar caps in the region of the fuselage frames were modeled using BAR elements
while the remainder of the spar caps and rib caps were simulated by CONROD elements.
Skin panels were represented by QDMEM2 members, although there were some triangu-
lar, TRMEM, membrane elements used to describe intricate corners. SHEAR elements
were used to represent the spar and rib webs.

Attachment of the rudder to the vertical fin was accomplished through two
hinges from the aft spar of the vertical fin to the leading edge of the rudder.
The hinge model consisted of a framework of eight CONRODs that connected the hinge
point to a rudder rib on the aft side and to a vertical fin rib on the forward
side. The first group of four CONRODs, or the aft hinge, connected the hinge point
to four points on the adjacent rudder rib, while the second group of four CONRODs,
or the forward hinge, connected the hinge point to four grid points on the adjacent
vertical fin rib (see figure 2). This method of modeling facilitated an easier
computation of hinge loads through a resolution of forces in the CONRODs into
forces in a predefined coordinate system by using a series of transformation equa-
tions. The torque load in the rudder was restrained by a bellcrank mounted on a
torque tube whose axis coincided with the hinge line of the rudder. This torque
tube was attached to the bottom of the rudder on one end and to a bracket support
on the aft side of frame 48 on the other end. BAR elements were used to model the
torque tubes and the bellcrank assembly which actuated and controlled the rudder
rotation at the bottom of the torque tube. Modeling of the bracket support on
frame 48 was accomplished using CONRODs for the stiffeners and QDMEM2 membranes
for the webs.

The horizontal tail consisted of the horizontal stabilizer and right hand and left hand elevators. Attachment of the horizontal stabilizer to the vertical fin was accomplished through a hinge point on the top of the vertical fin between spars three and four and a screwjack attached to the horizontal stabilizer apex and spar two of the vertical fin. Rotation of the horizontal tail could then be achieved through actuation of this screwjack. The elevators were attached to the rear spar of the horizontal stabilizer through three hinges on each side.

Three separate local rectangular coordinate systems were created using the CORD2R facility in NASTRAN to model the horizontal tail structure. These local coordinate systems were used to describe the horizontal stabilizer, right hand elevator, and left hand elevator. Layout of the horizontal stabilizer local rectangular coordinate systems was established with the origin located at the horizontal stabilizer apex with the X axis positive aft, the Y axis positive left hard outboard, and the Z axis positive down. Orientation of the left hand elevator local rectangular coordinate system was defined with the origin at the intersection of the hinge line and aircraft center plane with the X axis perpendicular to the hinge line and positive aft, the Y axis coincident with the hinge line and positive left hand outboard, and the Z axis perpendicular to the X-Y plane and positive down. The right hand elevator local rectangular coordinate system was similar to the left hand elevator with some differences in positive axes directions. The origin for the right hand elevator coordinate system was the same as the left hand elevator; however, the X axis was perpendicular to the right hand hinge line and positive forward, the Y axis coincided with the right hand hinge line and was positive right hand outboard, and the Z axis was perpendicular to the X-Y plane and was positive up. One important advantage of the separate coordinate systems for the elevators was the ease and improved flexibility of analyzing the elevators and horizontal stabilizer with the elevators in various deflected positions.

Grid points in the horizontal tail were specified in relation to the appropriate coordinate system depending on whether the point was in the horizontal stabilizer, right hand elevator, or left hand elevator. Location of the grid points was defined by the intersection of the spars and stringers with the ribs and by the exterior contour. As in the vertical fin, the spar caps, stringers and rib caps were represented by CONRODs, the spar and rib webs were SHEAR elements and the skin panels were modeled using QDMEM2 and TRMEM members in the horizontal stabilizer while QUAD2 and TRIA2 elements were used in the elevators. BAR elements were used to simulate the elevator trailing edges.

Attachment of the elevators to the horizontal stabilizer rear spar was accomplished by three hinges on each elevator. These hinges were designated by the spanwise location and were referred to as the inboard hinge, center hinge, and tip hinge (see figure 3). The center and tip hinges were modeled as a framework of eight CONRODs that connected the hinge point to an elevator rib and a horizontal stabilizer rib. The first group of four CONRODs, or aft hinge, connected the hinge point to four grid points on an elevator rib, while the second group of four CONRODs, or forward hinge, connected the hinge point to four grid points on a horizontal stabilizer rib (see figure 3). The torque load on the elevator was reacted by a bellcrank mounted on a torque tube whose axis coincided with the elevator hinge line. There were two of these bellcrank/torque tube assemblies, one for each side. The torque tube attached to the elevator on the tube's outboard

end and to a bracket support mounted on the horizontal stabilizer's rear spar on the airplane center line on the tube's inboard end. Both torque tubes and bellcranks were modeled using BAR elements, while the center line bracket support assembly was modeled using CONRODs.

CONTROL SYSTEM

A portion of the control system connecting the rudder and elevator has also been included in the modeling of the empennage section to more accurately define the effect of control system stiffness on the deflection of these control surfaces and in particular the associated hinge forces. Rudder motion on the Learjet M55 aircraft was accomplished by rudder pedal movement which was transferred by a closed loop cable assembly which drove a bellcrank mounted on the rudder torque tube (see figure 4). The aft portion of this cable system was included in the finite element model and was represented by CONROD elements with the side of the closed loop cable system that was not in tension removed. The CONROD elements representing the cables were extended into the tailcone section where the forward end of this member was attached to a pulley which was restrained against rotation.

Elevator deflection on this aircraft was achieved by control column movement which was transferred through a closed loop cable assembly and a push-pull rod linkage system. The upper portion of the push rod system consisted of two round tubes which were attached to the bellcranks on the left and right elevators respectively. The other end of these two push rods were joined to a down spring linkage mounted on the aft side of spar three in the vertical fin. A single round tube was used in the lower portion of the push rod system. This shaft was connected to the down spring linkage on the top end and to a sector on the bottom end (see figure 5). The portion of the elevator control system that was included in the empennage model consisted of the elevator bellcranks, upper push rods, down spring linkage, and lower push rod which was constrained at the lower end for the NASTRAN analysis. The grid points that defined the top and bottom points of the lower push rod were defined in separate local cylindrical coordinate systems. This was done so that these grid points could be moved with the elevator motion by using a simple set of transformation equations. The push-pull rods were modeled with CONRODs, whereas the bellcranks and down spring linkage were represented by an assemblage of BAR elements.

The horizontal stabilizer rotation about the hinge point between spar three and four on top of the vertical fin was achieved by a screwjack actuator attached to the horizontal stabilizer apex. A BAR element was used to represent the screwjack. One end of this BAR element was attached to a fitting on the forward side of spar two in the vertical fin, and the other end was connected to a fitting mounted on the horizontal stabilizer center line. The fittings that attached the screwjack actuator at both ends were also modeled using BAR elements.

LOADS AND CONSTRAINTS

Many different load conditions were analyzed using the NASTRAN empennage model. A correlation analysis was performed on the horizontal tail using a positive gust with top roll moment load condition from the 35/36 fatigue test spectrum. This load case was selected basically because earlier tests did not have sufficient instrumentation to perform a correlation analysis, and this particular case was one of the higher load conditions in the 35/36 fatigue test spectrum. Since the correlation analysis for the vertical tail was described in a previous NASA paper (See ref. 1), the results of that work were not presented here. The analysis of the Learjet 55 vertical tail described in this paper was directed mainly at rudder hinge force calculations. The load case applied to the vertical tail for these rudder hinge force calculations was a maximum side bending with rudder kick load condition.

NASTRAN runs were made for all of the 35/36 horizontal tail static test loads. These conditions were run in order to establish a baseline for the Model 55 analysis so that a determination could be made as to whether any of the 55 horizontal tail internal loads and stresses exceeded those on the 35/36 horizontal tail. Since some of the 35/36 load cases were tested to 150% ultimate load, there was good reason to believe that the 55 horizontal tail load conditions were covered by the previous 35/36 static tests. The 35/36 loads were applied to the horizontal stabilizer and elevators with the elevators in the neutral, or undeflected position, the 15° up position and the 15° down position. The loads definition for the Model 55 horizontal tail was somewhat different from the 35/36 horizontal tail. There were many more load cases for the Model 55 airplane than for the 35/36 airplane, and a direct comparison was not easily achievable for many of these conditions. Consequently, internal loads and stresses were determined for the 55 horizontal tail load conditions with the elevators in the undeflected and deflected positions using NASTRAN analysis in order to establish a common basis for comparison with the 35/36 internal loads and stresses.

Loads were applied to the vertical fin, rudder, horizontal stabilizer and elevators using FORCE card images (See ref. 2). These forces were applied at the grid points to simulate the shear, bending and torque envelopes for these airfoil surfaces. A computer program was written which accepted concentrated forces from the test loads data as input and redistributed these forces proportionately to the four nearest grid points according to the distance from those nodes and generated FORCE card images as output.

Constraints for the empennage model were applied at several locations. The majority of constraints were applied along the perimeter of frame 39 (See figure 2) in all three translational degrees of freedom at the frame and stringer intersections. Other constraints were applied to the rudder control system and elevator control system. The rudder control system was constrained by attaching the forward end of the tailcone rudder cable to a frame in the tailcone section. The elevator control system was restrained by using SPC, single point constraints, (See ref. 2) on the three translational degrees of freedom at the bottom end of the lower push rod (See figure 2).

Grid coordinates on the control surfaces were specified with respect to the appropriate rudder or elevator local rectangular coordinate system. These local coordinate systems were initially defined for the control surface in the undeflected position. However, the control surface could be deflected or rotated without changing the grid point coordinates merely by rotating the local coordinate system. This was accomplished by modifying the CORD2R card image in the bulk data deck by transforming the original axes reference to a new axes reference.

The CORD2R card image in the bulk data deck for each control surface defined a rectangular coordinate system by reference to three points. The first point "A" (A1, A2, A3) defined the origin of the local coordinate system (See figure 6). The second point "B" (B1, B2, B3) defined the direction of the "Z" axis, and the third point "C" (C1, C2, C3) defined a point in the X-Z plane. The basic coordinate system was used as the reference system for these points (See ref. 2). The origin for the basic system was defined at fuselage station (F.S.) 0.00, butt line (B.L.) 0.00, and waterline (W.L.) 0.00 with the "X" axis positive aft, "Y" axis positive left hand outboard, and the "Z" axis positive down. Components of A, B, and C were defined on the CORD2R card image by means of a simple series of transformations described by the following matrix equations.

$$\left[H_\theta \right] = \left[T_\theta \right] \times \left[H_L \right] \tag{1}$$

The equation shown above converts coordinates in a swept deflected control surface to coordinates in a swept undeflected control surface. Equation (2) shown below transformed the coordinates in equation (1) to coordinates parallel to a fuselage reference system corrected for the hinge line sweep angle λ.

$$\left[H_\lambda \right] = \left[T_\lambda \right] \times \left[H_\theta \right] \tag{2}$$

Substituting equation (1) into equation (2) and then referencing these values to the basic system with an H_{GO} matrix resulted in equation (3).

$$\left[H_G \right] = \left[T_\lambda \right] \times \left[T_\theta \right] \times \left[H_L \right] + \left[H_{GO} \right] \tag{3}$$

Equation (3) was used to calculate the components of points "B" and "C" on the CORD2R card which defined the rotated control surface.

HINGE LOAD CALCULATION

As indicated previously, the hinges were modeled using CONRODS and/or Bar elements. Since the hinge point had to be in equilibrium under the action of the internal element forces, the resultant of the forces from the elements on the aft side of the hinge line

must be equal and opposite to the resultant from the elements on the forward side of the hinge line. This force on the forward hinge member was defined as the hinge force for each of the control surface support points.

Internal forces in the CONRODs and BARs were extracted from the NASTRAN output for a given load case. The forces in the hinge elements were then rotated into a common coordinate system through a series of transformations (See figure 7). The three force components in the element coordinate system were then defined as F_{xE}, F_{yE}, and F_{zE}. Orientation of the element coordinate system was defined by the two end points of the member and a $\vec{v}$ vector, if the element was a BAR (See ref. 2). Element grid point components x_A, y_A, z_A and x_B, y_B, z_B (See figure 7) established the basis for transforming the element forces to a common coordinate system. This was accomplished by rotating, or transforming, these forces through three angles α, β, and γ. Upon calculation of these three rotations, the transformation matrices were formed as shown in figure 7. The element forces F_{xE}, F_{yE}, and F_{zE} were then resolved in the common X, Y, Z directions, and then the hinge force components were determined by summing the resolved individual element forces.

A small computer program was written to perform the transformation from the element coordinate system to the common reference coordinate system. This program also accounted for the effect of control surface rotation. Hinge loads were computed on both sides of the hinge line as a check on the transformation calculations. The hinge loads at all the hinge points plus the loads at the intersection of the torque tubes and bellcranks were also summed to check the equilibrium of these hinge loads with the control surface applied loads.

BUCKLING ANALYSIS

A comparison of skin cover compressive stresses with the corresponding panel buckling allowables indicated the presence of skin panel buckling for several load cases. Consequently, an automated buckling analysis was implemented to identify buckled skin panels and to simulate this non-linear phenomenon in the NASTRAN analysis. The buckling simulation was achieved by replacing the original skin thickness of the buckled panel with an effective skin thickness which represented the stiffness of the buckled configuration. A detail description of the theory for this analysis has been described in reference 3. The buckling analysis and effective skin thickness calculation were coded into a computer program which was set up to run as a post processor to the NASTRAN program. This NASTRAN analysis with the buckled effective skin thickness generally had to be repeated several times in order to obtain a convergent solution. Since some of the loading cases on the horizontal tail were combined conditions, the buckling analysis was performed on both the upper and lower surfaces simultaneously.

ANALYTICAL RESULTS

After extensive analysis and study, the applied loads on the Model 55 horizontal tail were determined to be less than the maximum tested loads on the 35/36 horizontal tail which was identical to the 55 in structural detail. Consequently, no static test was performed on this structure during the 55 testing program.

However, in order to establish a correlation between the horizontal tail portion of the NASTRAN empennage model and the structural test data, a positive gust condition with top roll moment load case was used from the Model 35/36 fatigue test program as was mentioned previously. The results of this test along with the NASTRAN data have been exhibited in figures 8 through 11. Figures 8 and 9 show the correlation on the horizontal stabilizer forward spar upper cap and lower cap respectively while figures 10 and 11 show the correlation on the rear spar upper cap and lower cap respectively. Most of the experimental points agree with the NASTRAN data very closely with the exception of the most inboard point on the rear spar lower cap. This gage was very near an access door in the skin panel and appeared to be affected by the stress gradient due to this cutout. As mentioned earlier, no correlation was presented on the vertical tail, since this was performed in an earlier paper (See ref. 1).

CONCLUDING REMARKS

A method has been demonstrated for calculating control surface hinge forces using a Learjet Model 55 empennage NASTRAN analysis. Hinge element internal forces were extracted from the NASTRAN analysis and converted to a common coordinate system using a set of transformation equations to define the individual hinge forces. Since each control surface was defined in a local rectangular coordinate system, rotation of the control surface could be easily accomplished by transforming the components on the CORD2R card. This control surface rotation capability permitted Learjet to investigate the impact of control surface movement on the hinge attachments in more detail than was previously possible. A buckling analysis was also performed to determine the non-linear effect of skin panel buckling on stringer and spar cap stresses. These techniques proved to be a valuable asset to Learjet in studying the structural operating characteristics of the Model 55 empennage structure and associated control surfaces and for substantiating the horizontal tail structure by comparison with previous tests.

REFERENCES

1. Boroughs, Robert R.; Paramasivam, Sivam; and Werner, Joanna K: Development and Analysis of the Learjet 54/55 Fuselage NASTRAN Model Using Substructure Techniques, Ninth NASTRAN user's Colloquium, NASA CP 2151, October 1980, pp. 201-223.

2. The NASTRAN User's Manual (Level 17.5), NASA SP-222 (05), Washington, D.C., December 1978.

3. Abla, Mike H.; Boroughs, Robert R.; and Cook, Everett L.: Analysis of The Learjet 35/36 Wing and Correlation With Experimental Results, NASTRAN User's Experiences, NASA TMX-3428, Otober 1976, pp. 331-352.
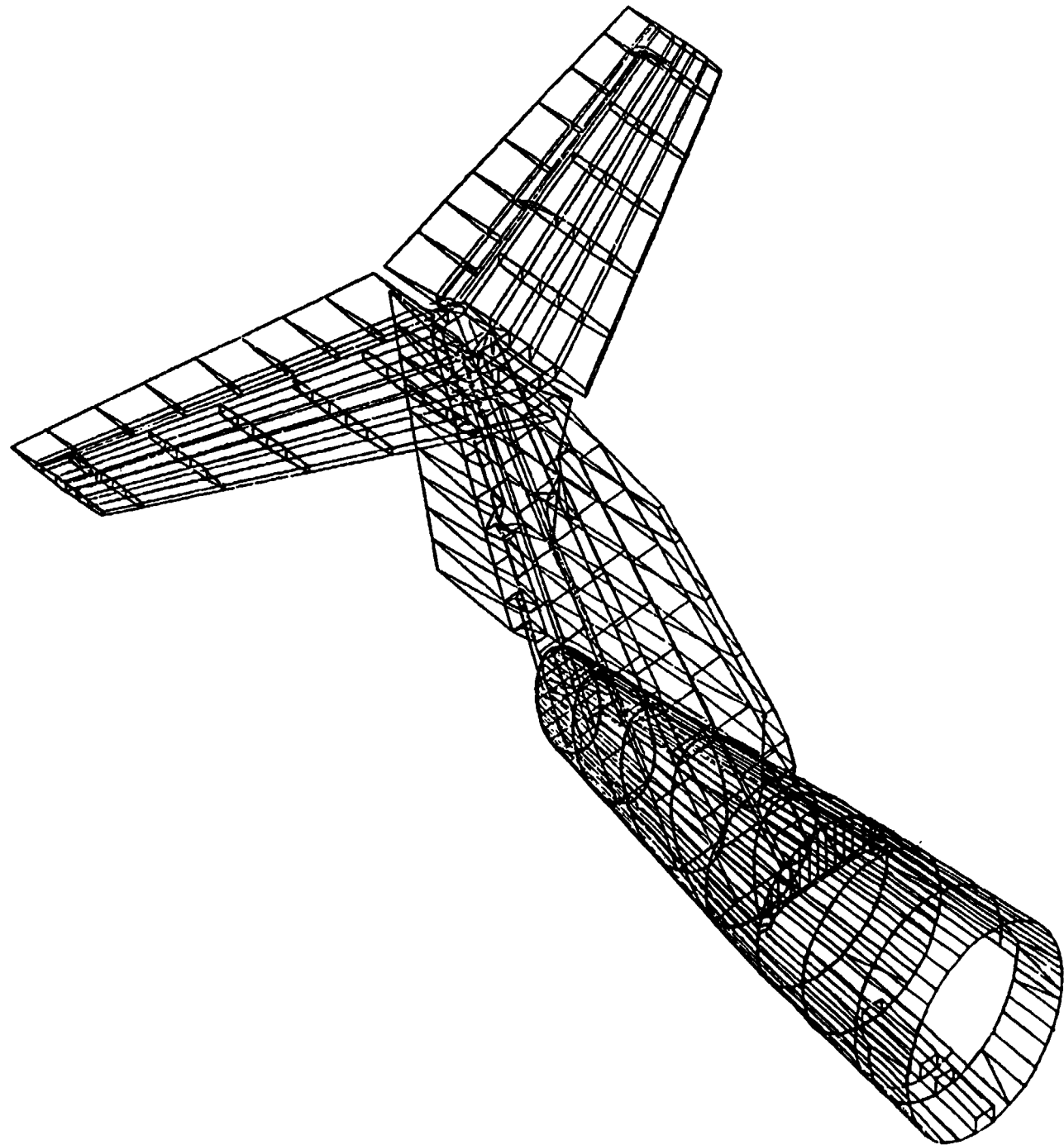
FIGURE 1 - NASTRAN 55 EMPENNAGE MODEL

Elevator Bellcrank

Horizontal Tail Screwjack Actuator

Elevator Upper Push Rods

Rudder
Top
Hinge

Elevator Lower Push Rod

Rudder
Center
Hinge

Rudder Torque Tube

Bracket Support
Assembly
(Rudder Bottom)
Hinge

Frame 48

Frame 41

Frame 39

FIGURE 2 - VERTICAL TAIL STRUCTURE

239

FIGURE 3 - HORIZONTAL TAIL STRUCTURE

FIGURE 4 - RUDDER CONTROL SYSTEM

FIGURE 5 - ELEVATOR CONTROL SYSTEM

ORIGINAL PAGE IS
OF POOR QUALITY

Input Data Card C∅RD2R   Rectangular Coordinate System Definition

Description: Defines a rectangular coordinate system by reference to the coordinates of three points. The first point defines the origin. The second point defines the direction of the z-axis. The third point defines a vector which, with the z-axis, defines the x-z plane. The reference coordinate must be independently defined.
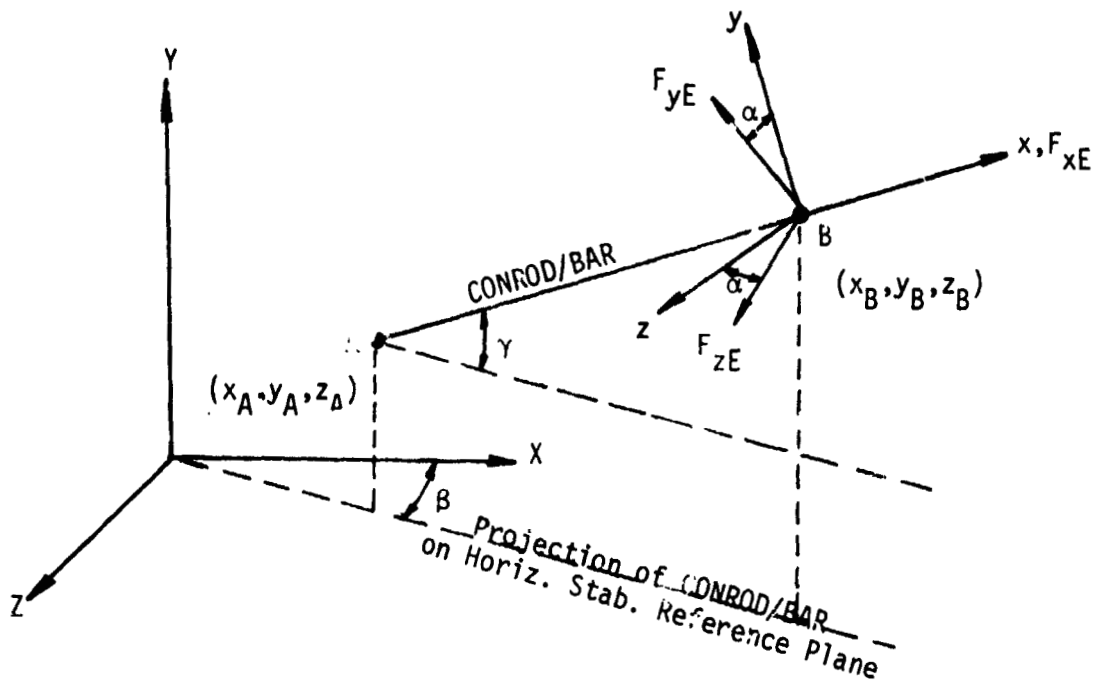

Format and Example:

1	2	3	4	5	6	7	8	9	10
C∅RD2R	CID	RID	A1	A2	A3	B1	B2	B3	ABC
C∅RD2R	3	17	-2.9	1.0	0.0	3.6	0.0	1.0	123

1	2	3	4						
+BC	C1	C2	C3						
+23	5.2	1.0	-2.9						

Field	Contents
CID	Coordinate system identification number (Integer > 0)
RID	Reference to a coordinate system which is defined independently of new coordinate system (Integer $\geq$ 0 or blank)
A1,A2,A3 B1,B2,B3 C1,C2,C3	Coordinates of three points in coordinate system defined in field 3 (Real)

Remarks: 1. Continuation card **must** be present.

2. The three points (A1, A2, A3), (B1, B2, B3), (C1, C2, C3) must be unique and non-collinear. Noncollinearity is checked by the geometry processor.

3. Coordinate system identification numbers on all C∅RD1R, C∅RD1C, C∅RD1S, C∅RD2R, C∅RD2C, and C∅RD2S cards must all be unique.

4. An RID of zero references the basic coordinate system.

5. The location of a grid point (P in the sketch) in this coordinate system is given by (X, Y, Z).

6. The displacement coordinate directions at P are shown by (u_x, u_y, u_z).

FIGURE 6 - CORD2R COORDINATE SYSTEM CARD IMAGE

$$
\begin{bmatrix} F_{XE} \\ F_{YE} \\ F_{ZE} \end{bmatrix} = \begin{bmatrix} \cos\beta & 0 & -\sin\beta \\ 0 & 1 & 0 \\ \sin\beta & 0 & \cos\beta \end{bmatrix} \begin{bmatrix} \cos\gamma & -\sin\gamma & 0 \\ \sin\gamma & \cos\gamma & 0 \\ 0 & 0 & 1 \end{bmatrix} \begin{bmatrix} 1 & 0 & 0 \\ 0 & \cos\alpha & -\sin\alpha \\ 0 & \sin\alpha & \cos\alpha \end{bmatrix} \begin{bmatrix} F_{xE} \\ F_{yE} \\ F_{zE} \end{bmatrix}
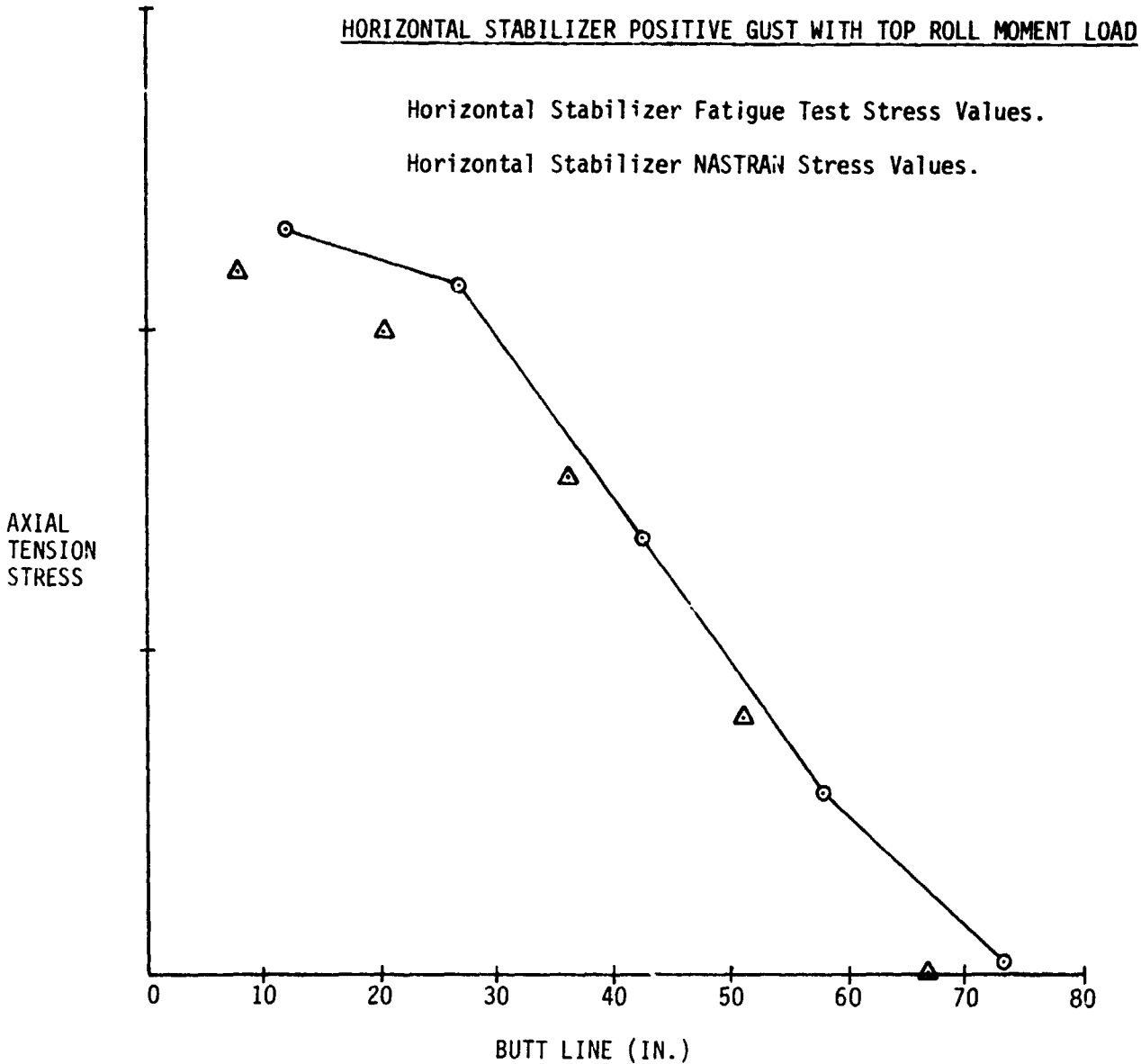$$

FIGURE 7 - HINGE FORCE TRANSFORMATION

FIGURE 8 - HORIZONTAL STABILIZ FORWARD SPAR UPPER CAP STRESSES

HORIZONTAL STABILIZER POSITIVE GUST WITH TOP ROLL MOMENT LOAD

Horizontal Stabilizer Fatigue Test Stress Values.
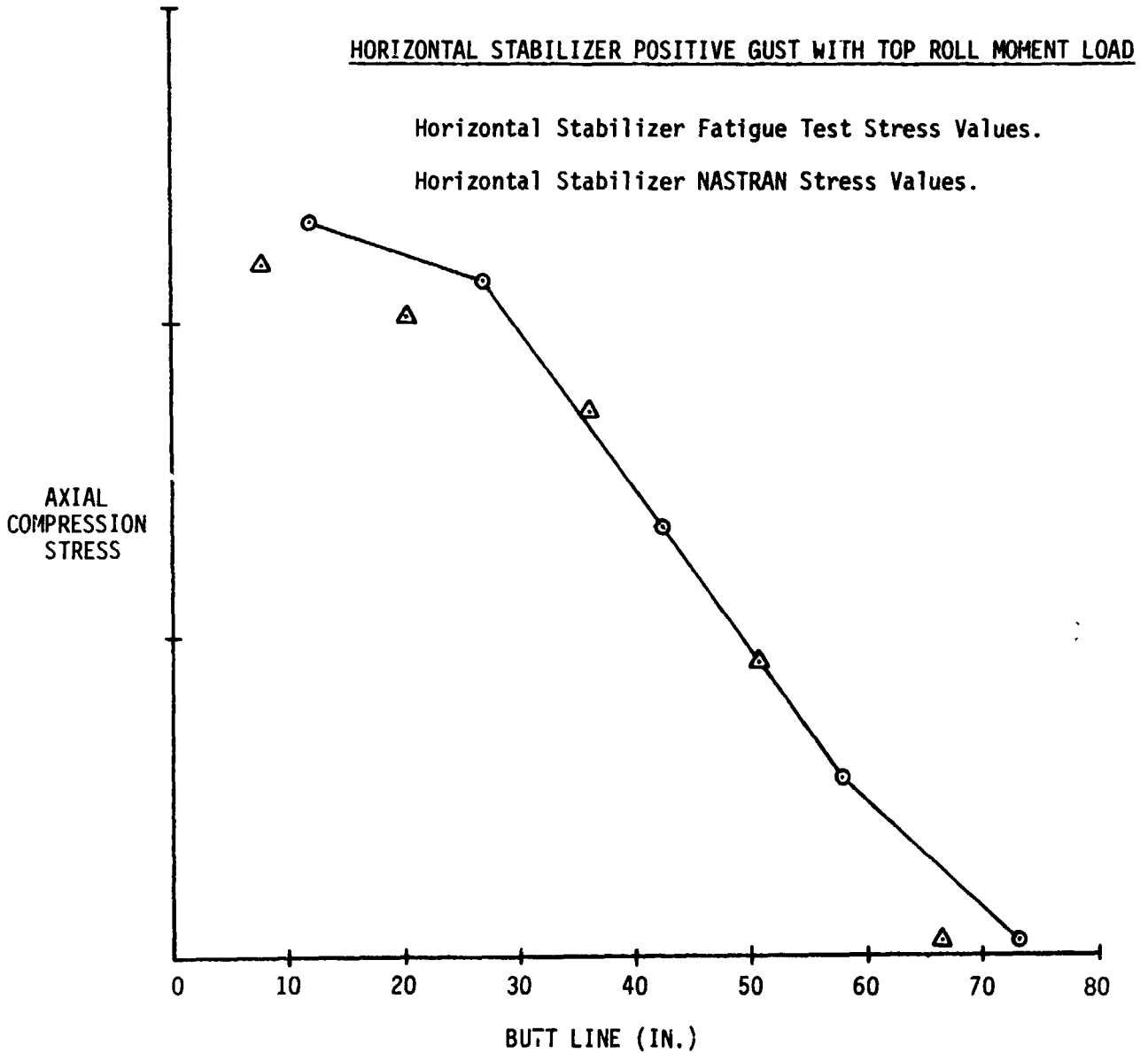
Horizontal Stabilizer NASTRAN Stress Values.

AXIAL
COMPRESSION
STRESS

BUTT LINE (IN.)

FIGURE 9 - HORIZONTAL STABILIZER FORWARD SPAR LOWER CAP STRESSES

HORIZONTAL STABILIZER POSITIVE GUST WITH TOP ROLL MOMENT LOAD

Horizontal Stabilizer Fatigue Test Stress Values.
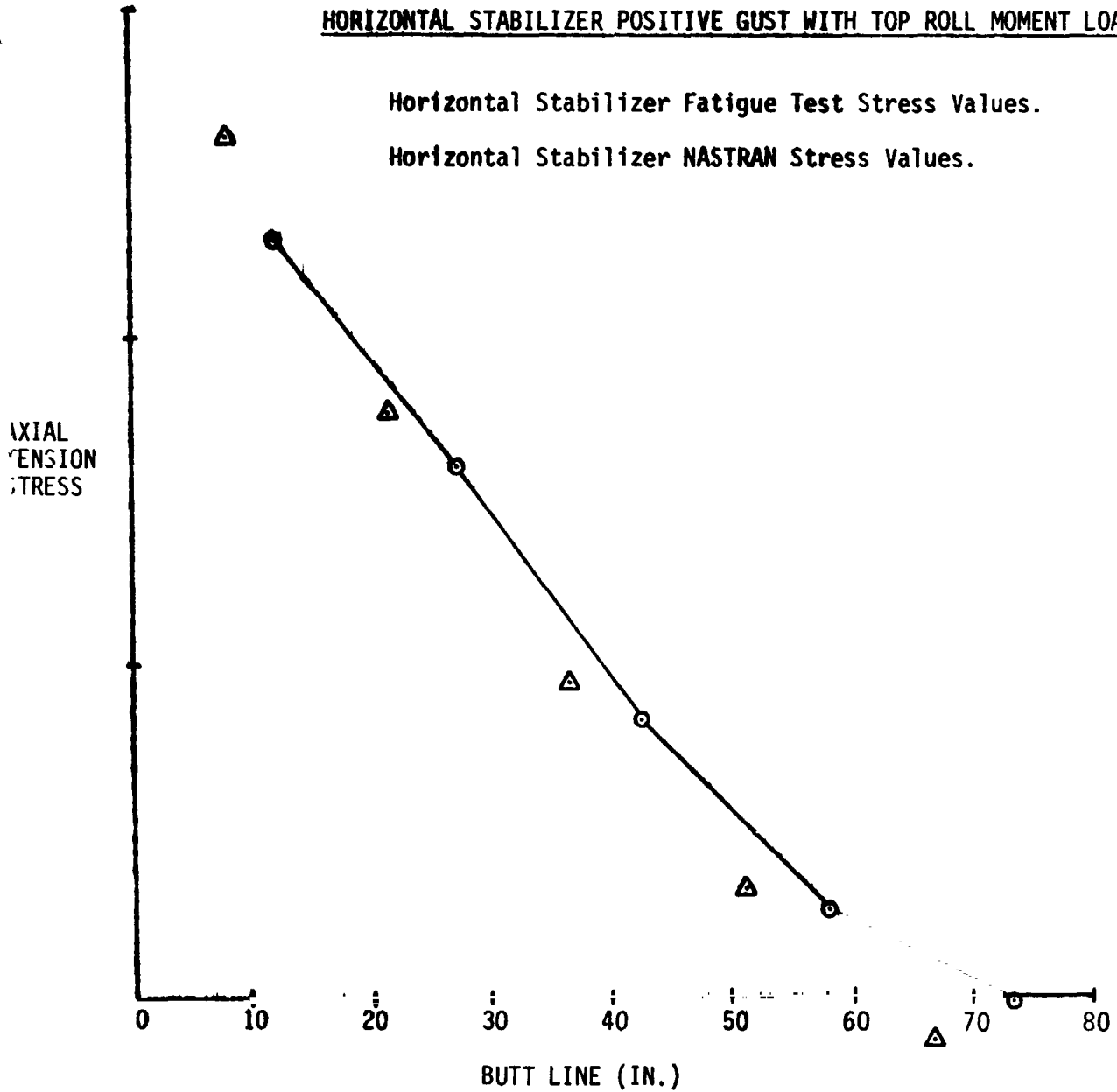
Horizontal Stabilizer NASTRAN Stress Values.

AXIAL
TENSION
STRESS

BUTT LINE (IN.)

FIGURE 10 - HORIZONTAL STABILIZER REAR SPAR UPPER CAP STRESSES

247

HORIZONTAL STABILIZER POSITIVE GUST WITH TOP ROLL MOMENT LOAD

Horizontal Stabilizer Fatigue Test Stress Values.

Horizontal Stabilizer NASTRAN Stress Values.

AXIAL
COMPRESSION
STRESS

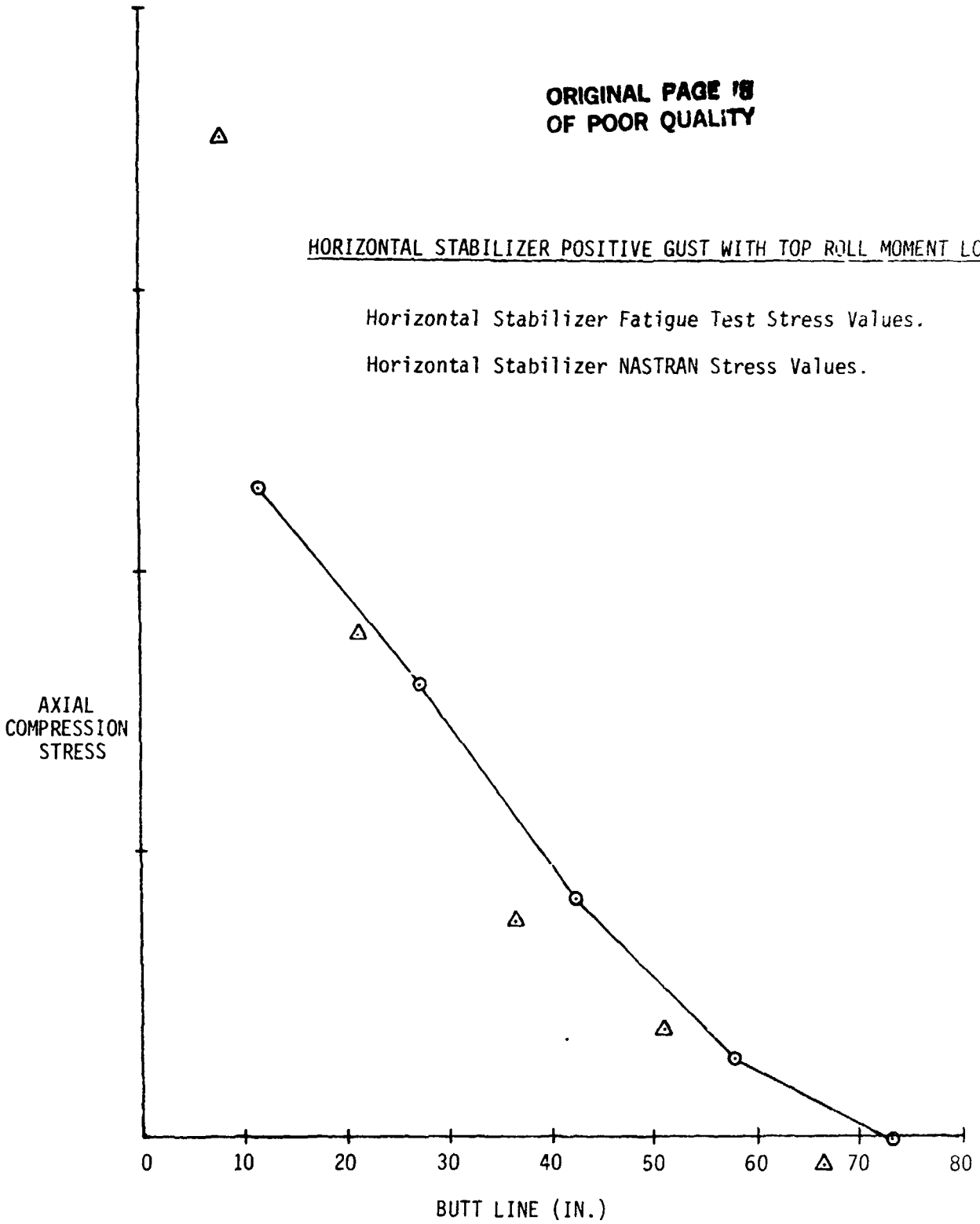0   10   20   30   40   50   60   70   80

BUTT LINE (IN.)

FIGURE 11 - HORIZONTAL STABILIZER REAR SPAR LOWER CAP STRESSES